ACS OMEGA

Open Access

http://pubs.acs.org/journal/acsodf

Article

Investigating the Acid Erosion Characteristics of Carbonate Rocks under Hydrodynamic Action

Jiaxin Zhang, Xuewei Chu,* Hai Fu, Qilin Zhang, and Shaokang Zong

Cite This: *ACS Omega* 2024, 9, 18922−18931

Read Online

ACCESS | Metrics & More | Article Recommendations

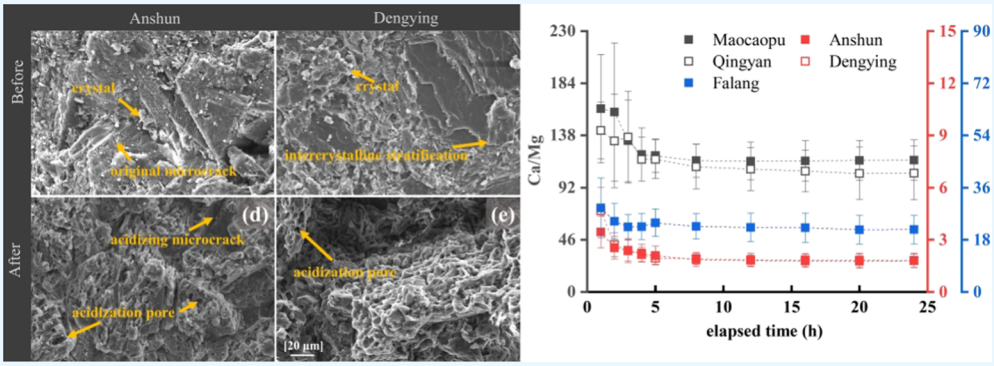

ABSTRACT: In carbonate areas, the unique dissolution features bring a lot of resistance to engineering constructions. The acidic filtrate will definitely cause accelerated dissolution of the surrounding rocks, and the mechanism of accelerated dissolution of such rocks in acid is not clear. In order to explore the dissolution pattern of carbonate rocks after the alteration of their primary environments, a self-made rotating reaction device was used to conduct laboratory dissolution experiments on carbonate cores under three conditions. The mass loss, the change of pH, the molar concentration of Ca^{2+} and Mg^{2+}, and the morphological changes before and after acid erosion were obtained. The results of correlation analysis show that the dissolution characteristics of carbonate are significantly related to dissolution time, composition of rocks, liquid flow rate, and acid concentration. Segmented characteristics were recorded between CaO/MgO and the reaction sequence (m). When 2 < CaO/MgO < 30, the increase of CaO/MgO has a significant contribution to the chemical dissolution rate; however, when 30 < CaO/MgO < 66, the increase of CaO/MgO does not contribute significantly to the chemical dissolution rate. The dissolution rate is positively correlated with the liquid flow rate. Also, liquid flow rate changes affect dolomite more than they do limestone. The mass loss rate (R_c) order of the rocks of the five carbonate formations was Maocaopu > Qingyan > Falang > Anshun > Dengying. Differences in dissolution induced by the acidic fluids in different formations will eventually form complex dissolution channels.

1. INTRODUCTION

The impact of acid leakage in karst areas is very prominent and has caused a great burden on the ecological environment. At the same time, various undesirable geological environmental problems have arisen. Acid mainly comes from landfills, slag landfills, and acid rain.[1−5] More specifically, the leakage of acidic liquid has caused pollution of the groundwater system and significantly accelerates the changes in the rock structure, mineral composition, pore structure, and mechanical properties in the acid etching area. These changes will lead to various problems, such as the foundation of the rock's strength and the leakage of the foundation of the rock.[6,7] Therefore, acidic liquid leakage will accelerate the erosion effect in the rock-soluble areas. The base rock around the filling area may also lead to the formation of a cycle of erosion and leakage. In this context, the impact of further exploring the lymation of acid liquid on carbonate rock is important and is considered to be of great significance in analyzing the stability and safety of the tailings and filling places.

Different types of acid−rock reaction experiments have been carried out in the literature to study and control the dissolution of soluble rocks. Remarkable results have been achieved on key issues, such as slowing or speeding up the acid−rock reaction rate. Many works have focused on controlling or changing the influencing factors of the reaction (acid concentration, temperature, rotational speed, lithology, and partial pressure of CO_2) so

Received: November 10, 2023
Revised: March 27, 2024
Accepted: March 28, 2024
Published: April 22, 2024

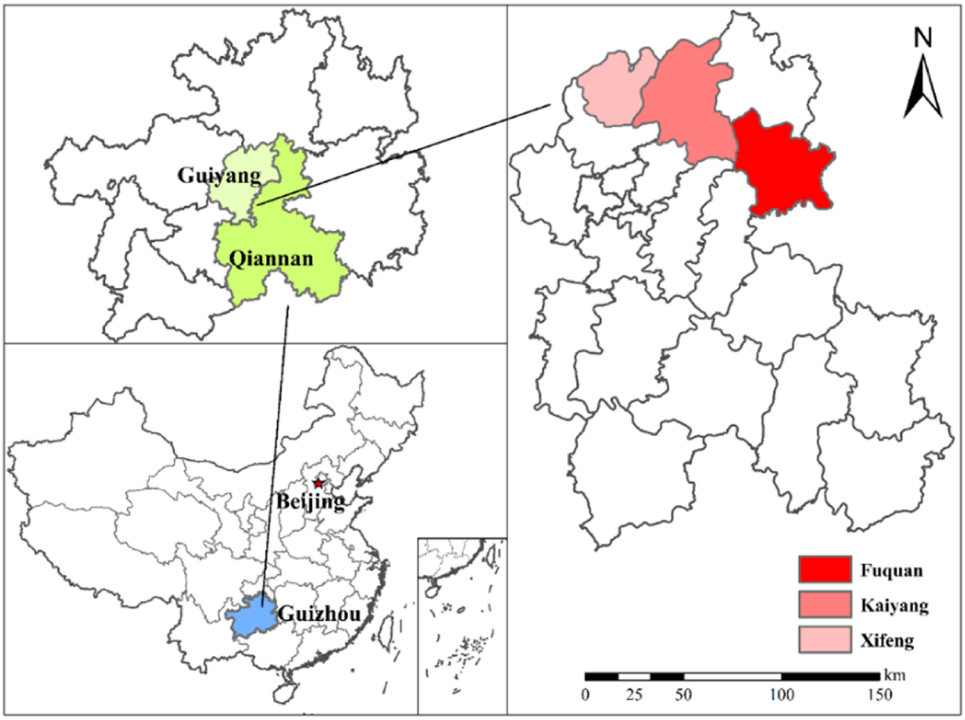

Figure 1. Overview map of the geographical location of the research area.

that the kinetic parameters, such as acid−rock reaction rate, H^+ consumption rate, reaction activation energy, reaction rate constant, and H^+ effective mass transfer coefficient can be changed during the dissolution process.[8−13] Experimental works have demonstrated that under the action of the hydrodynamic pressure, the dissolution of carbonate rocks mainly occurs outside the surface of the rock, and the voids inside the rock continue to deepen.[6,14] The correlation between the pore size distribution and the diffusion coefficient has been analyzed, suggesting that the dissolution rate and diffusion coefficient of limestone are affected by the pore size distribution, whereas the influence of porosity and permeability is inferior to that of the pore size distribution.[15] Other works have shown that the diffusion coefficient of hydrogen ions is affected by the flow rate of the acid solution, and the acid−rock reaction rate can be significantly accelerated by increasing the concentration of the acid solution, reaction temperature, and flow rate.[16,17] $CaCO_3$ and $MgCa(CO_3)_2$ are the main mineral components of carbonate rocks, and the release patterns of calcium and magnesium ions are regular. Interestingly, the release of Ca is always prior to that of Mg to reach a stable state. The analysis of the various changes, such as carbonate rock crystals, pore structure, and microcracking diversion capabilities, is usually performed from a microscopic angle.[5,18−22] Carrying out the rotating disk experiment,[17] it was proven that the dissolution quality is positively correlated with the dissolution volume and the acid−rock reaction rate. The main controlling factors of the surface dissolution morphology in the parallel and perpendicular directions of the acid flow are the acid−rock reaction rate and mineral composition distribution, respectively. At present, the majority of the reported works in the literature have examined the dissolution characteristics of carbonate rocks under single-factor conditions. Nonetheless, the dissolution mechanism under multifactor conditions has been scarcely reported. Along these lines, in this work, an indoor dynamic dissolution simulation experiment was carried out to study the dissolution mechanism of the different carbonate rocks after the original burial environment was changed. On top of that, the surface dissolution characteristics and chemical dissolution characteristics of carbonate rocks were thoroughly explored to clarify the hydrodynamic conditions and acid conditions, as well as the dissolution rate characteristics of carbonate rocks under joint action.

2. MATERIALS AND METHODS

2.1. Experimental Materials. *2.1.1. Carbonate Sample.* Guizhou Province in China is a typical karst mountain area, and most of the tailings reservoirs are located in karst valleys. If the antiseepage treatment of such types of storage areas is not appropriate, leakage often occurs. The leaching filtrate of some stored tailings is acidic, which not only affects the surrounding water environment but also accelerates the dissolution of carbonate rocks.

In this work, five different carbonate rock stratas located in Baiji Village, Fuquan City, Jiaoyishan in Xifeng County, and Longjingwan in Kaiyang County were selected as research objects within the scope of leaching filtrate leakage in three phosphogypsum stack dumps (Figure 1). The samples included limestone of the Lower Triassic Maocaopu Formation (T_1m), dolomite of the Anshun Formation (T_1a), limestone of the Middle Triassic Qingyan Formation (T_2q^2), limestone of the Falang Formation (T_2f^2), and dolomite of the Late Aurora Dengying Formation (Z_2dy). A fresh cylindrical core sample with a diameter of 25 mm and a height of 50 mm was drilled. Each stratum was screened for six pieces according to the appearance, morphology, chemical composition, and mineral composition similarity characteristics of the sample. A total of 30 rock samples exist in five groups of strata. Before the experiment, the rock samples were fully rinsed with deionized water and dried at 105−110 °C for 72 h.

https://doi.org/10.1021/acsomega.3c08557
ACS Omega 2024, 9, 18922−18931

Table 1. Test Results of the Main Compounds and Mineral Composition Content

	compound content			minerals, %				
strata	CaO, %	MgO, %	CaO/MgO	calcite	dolomite	quartz	plaster	type
Maocaopu	51.26	0.78	65.59	96.72	0.04	2.75	0.49	limestone
Qingyan	54.93	0.91	60.14	94.15	3.69	2.15		limestone
Falang	53.58	3.01	17.83	47.22	51.93	0.85		lime dolomite
Anshun	43.01	13.33	3.23	0.28	99.65		0.06	dolomite
Dengying	24.10	11.54	2.09		85.09	14.91		siliceous banded dolomite

The mineralogical composition of the sample was determined by performing X-ray diffraction (XRD) measurements. The chemical components of the sample are determined by using an X-ray fluorescence spectrum analyzer (XRF). Carbonate rock types were classified according to the relative content of calcite and dolomite. The test results of the main compounds and mineral composition content are presented in Table 1. The X-ray diffraction analysis showed that sample M contained 96.7% calcite and 2.7% quartz, sample Q contained 94.1% calcite, 3.7% dolomite, and 2.1% quartz, sample F contained 47.2% calcite and 51.9% dolomite, sample A contained 99.6% dolomite, and sample D contained 85.09% dolomite and 14.9% quartz. Both samples M and Q were extremely pure limestone; sample F was lime dolomite; sample A was pure dolomite; and sample D was dolomite sandwiched with siliceous rocks.

2.1.2. Acid Fluid. The pH values of the leaching filtrate of three phosphogypsum stack dumps were measured in the range of 1.12−2.64. Hydrochloric acid was used as the reaction medium in this work to simplify the reaction process and to avoid other ions from affecting the test process, such as ion effects.

2.2. Experimental Method. *2.2.1. Dynamic Dissolution Experiment.* To analyze the influence of hydrodynamic conditions on the acid erosion of carbonate rocks, a self-made rotating rock plate reactor was used to carry out dynamic dissolution simulation experiments at room temperature and pressure conditions (Figure 2).[15,23] The hydrochloric acid solution with a concentration of 67% was diluted with deionized water, and the acid solution with two concentrations of pH 1 and 2 was configured. The capacity of each group of the acid solution was 3500 mL. The sample rotated at a rate of 200, 400, and 600 rpm at the two acid concentrations of each stratum, corresponding to flow rates of 0.263, 0.523, and 0.785 m/s.

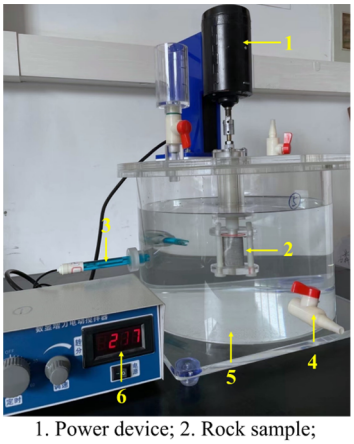

1. Power device; 2. Rock sample;
3. pH probe; 4. Liquid sample outlet;
5. Solution; 6. Speed regulator.

Figure 2. Self-made rotating rock plate reactor.

The timing has been timed since the acid−rock contact, at 0, 1, 2, 3, 4, 5, 8, 12, 16, 20, and 24 h, collect the solution. Each time, 30 mL of the reaction solution was collected, and the same volume of deionized water was added after sampling to maintain the volume of the solution. Because the volume of the water sample accounted for only 0.86% of the total volume of the reaction solution, the impact was negligible. The experiment was stopped after 24 h of reaction, and the rock sample was taken out and dried for 72 h to calculate the amount of core dissolution. The experimental design is shown in Table 2.

Table 2. Experimental Design

	flow rate		
initial pH	200 rpm	400 rpm	600 rpm
1	M1	M2	M3
	Q1	Q2	Q3
	F1	F2	F3
	A1	A2	A3
	D1	D2	D3
2	M4	M5	M6
	Q4	Q5	Q6
	F4	F5	F6
	A4	A5	A6
	D4	D5	D6

2.2.2. Analysis Method. Three parameters of mass loss percent (R_c), chemical dissolution rate (R), and acid−rock reaction rate were defined to quantitatively reflect the dissolution process and dissolution characteristics of carbonate rocks.

$$R_c = \frac{W_1 - W_2}{W_1} \times 100\% \quad (1)$$

where R_c is the mass loss percent (%), W_1 is the dry mass of the sample before the experiment (g), and W_2 is to the dry mass of the sample after the experiment (g).

$$R = \frac{2.5X + 3.5Y}{t} \quad (2)$$

where R is the chemical dissolution rate ($mg{\cdot}D^{-1}{\cdot}L^{-1}$), X is the content of Ca in the dissolution solution ($mg{\cdot}L^{-1}$), Y is the content of Mg in the dissolution solution ($mg{\cdot}L^{-1}$), and t is the elapsed time (D).

$$J = KC^m \quad (3)$$

where J is the chemical response rate at time t ($mol{\cdot}L^{-1}{\cdot}s^{-1}$), C is the acid concentration at time t ($mol{\cdot}L^{-1}$), K is the reaction speed constant ($(mol{\cdot}L^{-1})^{-m+1}{\cdot}s$), and m is the reaction sequence.

https://doi.org/10.1021/acsomega.3c08557
ACS Omega 2024, 9, 18922−18931

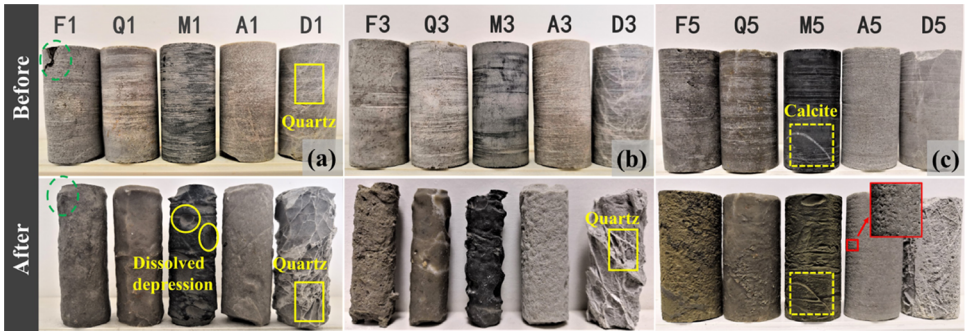

Figure 3. Morphological comparison of some rock samples before and after acid dissolution (a) at pH 1 and 200 rpm, (b) at pH 1 and 600 rpm, and (c) at pH 2 and 400 rpm.

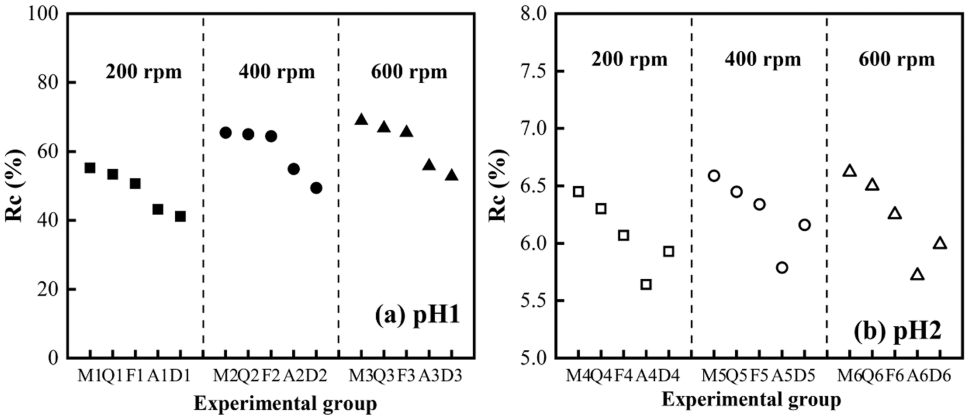

Figure 4. Mass loss percent (R_c) of the samples.

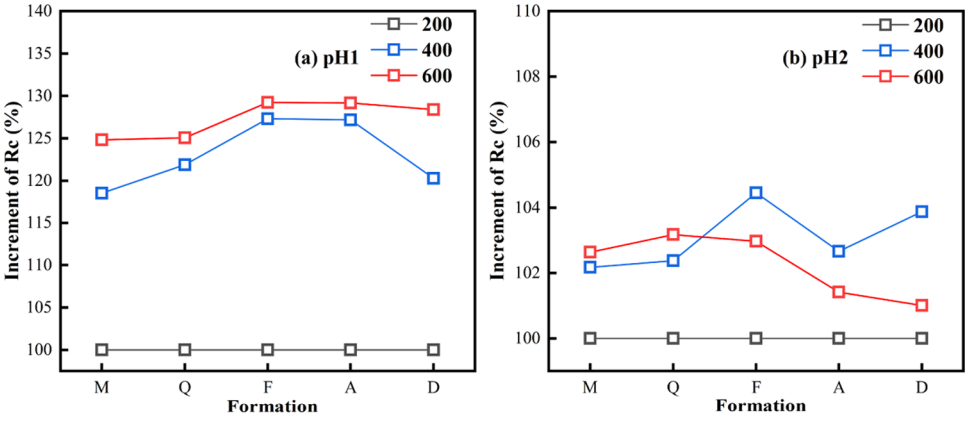

Figure 5. Increment of the mass loss rate (R_c) of the strata at 400 and 600 rpm based on the flow at 200 rpm.

3. RESULT

The based dissolution data of carbonate rocks were obtained by an atomic absorption test, SEM test, and pH test.

3.1. Rock Surface Morphological after the Acid−Rock Reaction. *3.1.1. Morphological Changes of the Sample.* After carrying out the dynamic dissolution experiment, to observe the surface morphology characteristics of the rock samples in various strata, three representative groups of samples were selected, which are shown in Figure 3. These included samples under experimental conditions of pH 1 and 200 rpm (a), pH 1 and 600 rpm (b), and pH 2 and 400 rpm (c). After being subjected to acid etching, the volume and surface morphology of the sample underwent significant changes. As can be observed in Figure 3a, the original crack in the upper left corner of F1 and the gap in the lower left corner of A1 were severely corroded by acid, and a significant depression compared to other uniform parts was detected. In the Q3 and Q5 samples shown in Figure 3b,c, the impurities were exposed and dissolution pits around them can be observed. There are dissolution pits on the surface of the M1, M3, and M5 samples, and the calcite veins on the surface of the M5 samples were preferentially dissolved. After the D1, D3, and D5 samples were dissolved, reticulated quartz veins were distributed on the surface. These quartz veins were extremely fragile and could easily be stripped off the surface of the rock sample. Compared with other strata, the surfaces of the M and Q samples were smoother after dissolution.

Figure 4 illustrates the mass loss percent (R_c) of each group of samples under different conditions, and the abscissa is the

https://doi.org/10.1021/acsomega.3c08557
ACS Omega 2024, 9, 18922−18931

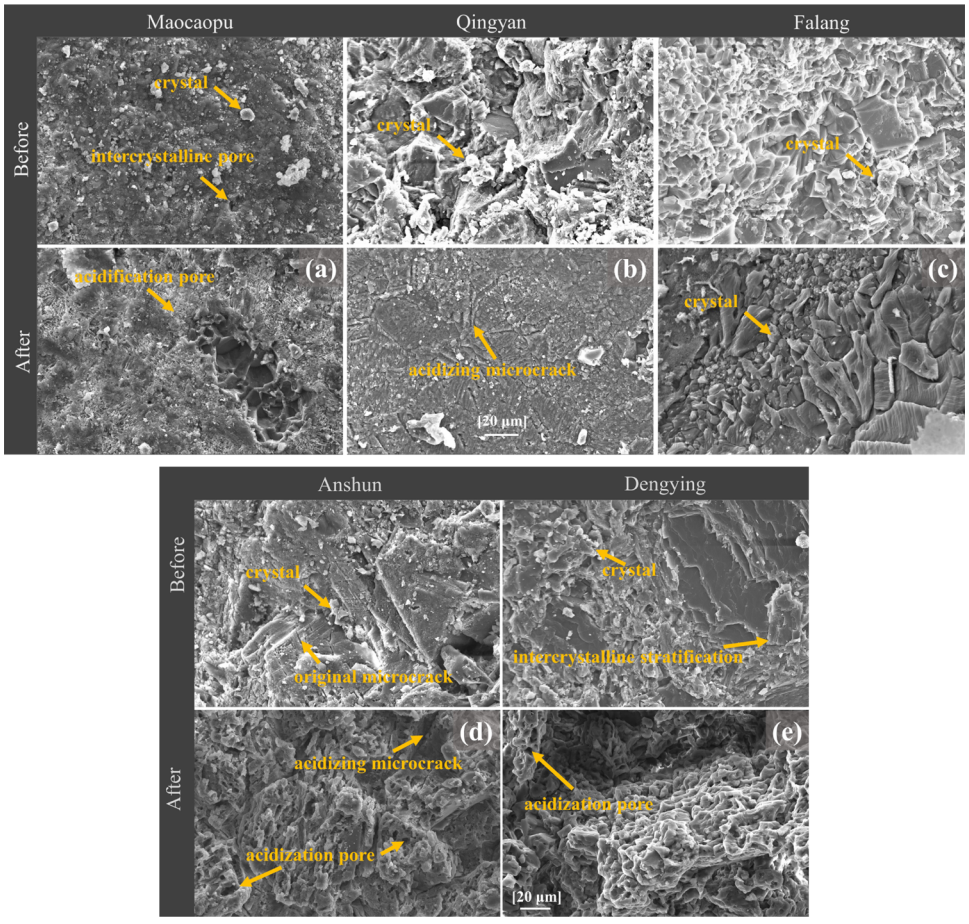

Figure 6. Microstructure of the samples' surface before and after acid dissolution: (a) Maocaopu, (b) Qingyan, (c) Falang, (d) Anshun, and (e) Dengying.

number of each experimental group. The dissolution rate R_c under pH 1 conditions exceeded 40%, and it exceeded 5% under pH 2 conditions. The R_c values of the first three groups of strata were all expressed as M > Q > F. Under pH 1 conditions, the R_c value was expressed as A > D (Figure 4a); under pH 2 conditions, it was expressed as D > A (Figure 4b).

Figure 5 shows the increment of the mass loss percent (R_c) of the strata at 400 and 600 rpm based on 200 rpm. Particularly, in Figure 5a, it is indicated that with the increase in the hydrodynamic conditions, the R_c of each group of samples was increased to a certain extent. At pH 1, the rotation speed was increased from 200 to 400 rpm, and the increment of the mass loss rate of the two F (27.30%) and A (27.16%) samples was greater than that of the M (18.52%), Q (21.87%), and D (20.25%) samples. The rotation speed was increased from 400 to 600 rpm, and the increment of the mass loss rate of the two groups of samples F (1.95%) and A (1.99%) was smaller than that of the samples M (6.30%), Q (3.20%), and D (8.14%). When the disk speed was increased from 200 to 400 rpm, the increment of the mass loss percent of Group F was still the highest. At pH 2, the mass loss percent of some samples did not increase with the increase in the hydrodynamic conditions (Figure 5b). When the disk speed was increased from 200 to 400 rpm, the increment of the mass loss percent of sample F was still the highest. From 400 to 600 rpm, only the mass loss percent of pure limestone in samples M and Q increased, while the mass loss percent of samples in samples F, A, and D decreased by 1.24−2.87%.

3.1.2. SEM Observation. A scanning electron microscope (SEM) was also used to observe the microstructure of the sample surface before and after the dissolution. The sample was made into small round pieces with a diameter of 1 cm and a thickness of 1−2 mm. After gold spraying, it was observed in the field of view of a 1000-fold electron microscope. An illustration of the pristine and the reacted samples' surface topographies was provided by the SEM images in Figure 6. Before being acidized, the original samples exhibited micropores but a few cracks. After acidizing, an elevated number of cracks were generated. However, their dissolution patterns were completely different. The surface crystal shape of Group M sample (a) was neat, with upright clusters of crystals, and the number of pores increased. After acid dissolution was performed, the crystals of sample M (a) were arranged in upright clusters. Sample Q (b) dissolved into more obvious staggered microcracks. The crystals of sample F (c) were attached in flakes. Furthermore, the original cracks in samples A and D (d, e) deepened, and the connection between the crystals weakened. The surface of the specimens was uneven and easily peeled off.

3.2. Evolution of the pH Value. Figure 7 displays the evolution of the pH values of the experimental solution at 200, 400, and 600 rpm. The pH value of each group of solutions continuously evolved with the reaction time. At different speeds, the pH of the samples M, Q, and F increased by 0.88−3.52, 1.81−5.00, and 4.92−5.02, respectively. The pH of samples A and D increased by 0.56 and 0.86, 0.79 and 1.62, and 0.87 and 1.51, respectively. In the pH 1 solution, the disk speed increased

https://doi.org/10.1021/acsomega.3c08557
ACS Omega 2024, 9, 18922−18931

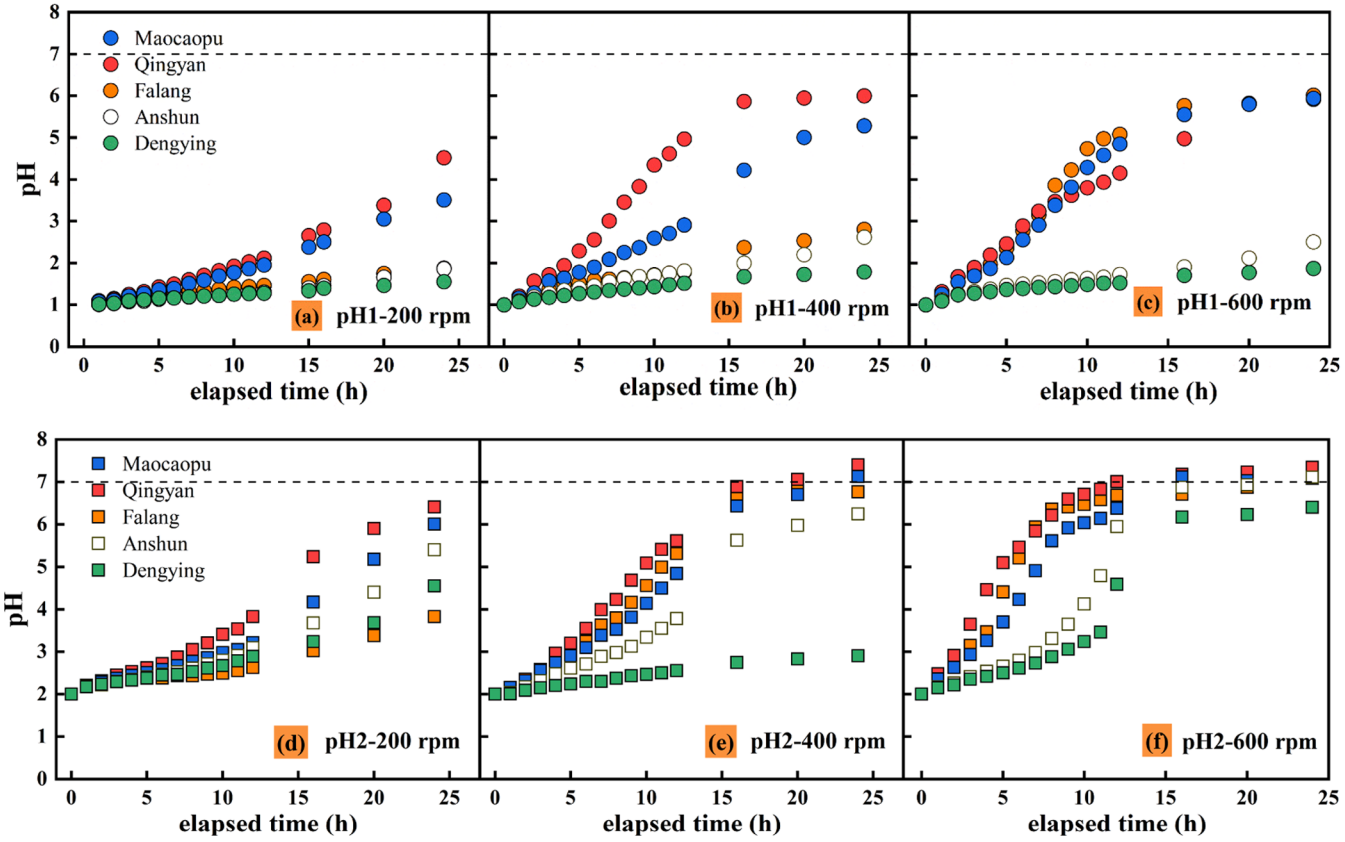

Figure 7. Evolution of the pH value of the experimental solution at 200, 400, and 600 rpm.

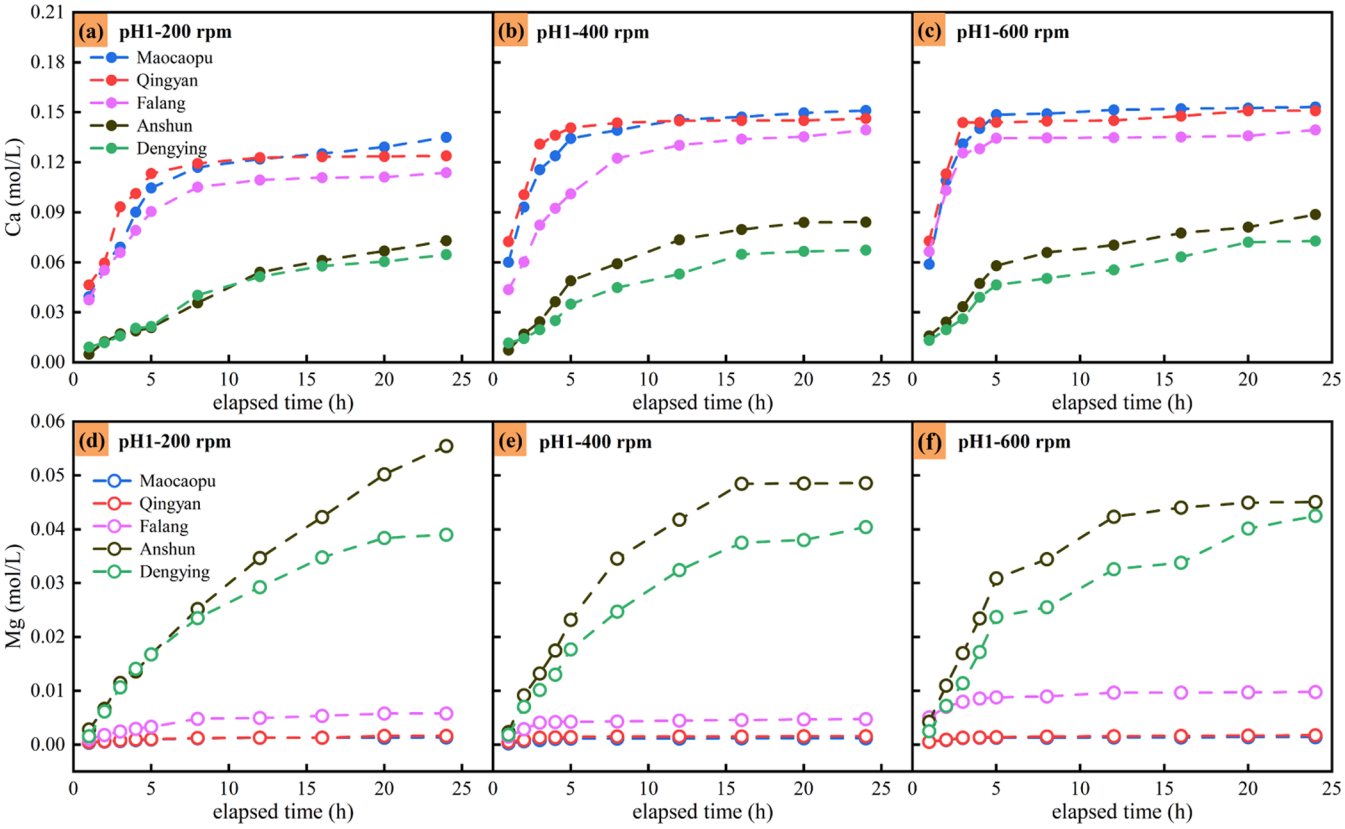

Figure 8. Concentrations of Ca and Mg released by the dissolution of the five samples plotted as a function of the time and the release characteristics.

https://doi.org/10.1021/acsomega.3c08557
ACS Omega 2024, 9, 18922−18931

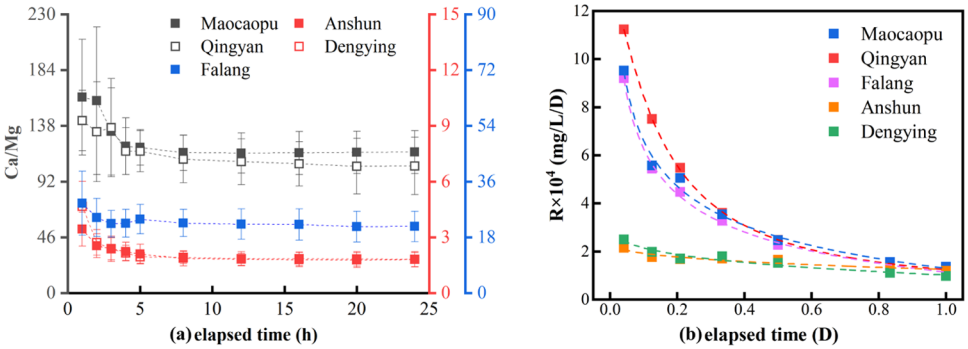

Figure 9. (a) Evolution of the Ca/Mg molar ratio in the dissolution of samples from five strata. (b) In the pH 1 solution, the chemical reaction rate (R) of each group of samples.

Table 3. Reaction Rate Constants at 200 and 400 rpm for Different Strata at pH 2

series	stratum	CaO/MgO	rotating speed (rpm)	K, $\times 10^{-6}$	J	R^2
α	M	65.59	200	0.964	$9.638 \times 10^{-7}\ C^{0.73}$	0.6804
	Q	60.14		1.107	$1.107 \times 10^{-6}\ C^{0.66}$	0.8751
β	F	17.83		1.023	$1.023 \times 10^{-6}\ C^{0.50}$	0.7686
γ	A	3.23		0.142	$1.418 \times 10^{-7}\ C^{0.38}$	0.8382
	D	2.09		0.051	$5.129 \times 10^{-8}\ C^{0.23}$	0.8214
α	M	65.59	400	3.928	$3.928 \times 10^{-6}\ C^{0.81}$	0.9204
	Q	60.14		9.312	$9.312 \times 10^{-6}\ C^{0.91}$	0.9430
β	F	17.83		9.308	$9.308 \times 10^{-6}\ C^{0.90}$	0.9258
γ	A	3.23		1.302	$1.302 \times 10^{-6}\ C^{0.69}$	0.8120
	D	2.09		1.069	$1.069 \times 10^{-6}\ C^{0.53}$	0.8756

from 200 to 600 rpm, and the pH values of samples M, Q, and F increased by 1.40−4.14, those of samples A and D only increased by 0.29−0.37, and those of the first three groups were 3.78−14.28 times those of the two groups.

3.3. Ca and Mg Release Characteristics. The concentrations of Ca and Mg released by the dissolution of the five samples were plotted as a function of the time and the release characteristics, as can be seen in Figure 8. At the initial acid pH of 1 or 2, the release of Ca and Mg increased with the reaction time. A significant correlation between the reaction time and the release amount ($R^2 \geq 0.977$) was detected. Overall, in pH 1 and pH 2 solutions, the Ca and Mg releases of M, Q, and F samples increased rapidly within 0−5 h. They were in a slow-increasing stage within 5−8 h, and they reached a relatively stable state in 8−24 h.[24] The release of Ca and Mg in samples A and D also rapidly increased within 0−5 h. Nonetheless, within 5−24 h, it basically showed uniform or small deceleration release characteristics and occasionally increased.

The characteristics of Ca release in each stratum under pH 1 conditions are also provided. The Ca release of the M sample was 0.135 mol/L, 0.151 mol/L, and 0.153 mol/L at 200, 400, and 600 rpm, respectively. The release of Ca in the F sample was 0.114 mol/L at 200 rpm and 0.140 mol/L at 400 and 600 rpm. The Ca release amount of sample D was 0.065 mol/L at 200 rpm, and the release amounts were 0.067 and 0.073 mol/L at 400 and 600 rpm, respectively. The evolution of the Ca/Mg ratio in the dissolution of samples from five strata is reported in Figure 9a. In the first stage of the reaction, the release rate of Ca was much higher than that of Mg, and then the Ca/Mg mole ratio tended to stabilize.[25]

3.4. Reaction Rate Constant (K). The reaction rate constant (K) increased with the increase in the CaO/MgO (%) ratio and R^2 = 0.9985. According to the difference in the CaO/MgO ratio, the five groups of strata were divided into three series: α (Maocaopu, Qingyan), β (Falang), and γ (Anshun, Dengying). The acid−rock reaction rate constant (K) under different conditions is given in Table 3. At 200 rpm, sample F had a CaO/MgO ratio of 17.83 and a reaction rate constant of 0.964×10^{-6}. Sample M had a CaO/MgO ratio of 65.59 and a reaction rate constant of 1.023×10^{-6}. The difference between the K values was 5.9×10^{-8}, while at 400 rpm, the difference in K values was 5.38×10^{-6}. The K value differs by 2 orders of magnitude between 200 and 400 rpm. When the hydrodynamic force is strong, the reaction rate constant shows a significant difference. The K values of sample D were 0.051×10^{-8} and 1.069×10^{-6} at 200 and 400 rpm, respectively.

4. DISCUSSION

The dissolution characteristics of natural rocks are affected by complex factors. Changes in the native environment of the rocks may accelerate uneven dissolution of the underlying surface. In this work, indoor dissolution experiments on samples from five carbonate formations were performed to explore the influence of leachate leakage in hydrochloric acid solutions at 200, 400, and 600 rpm and pH 1 and pH 2, respectively. The results indicated the relationship among the rock dissolution rate, dissolution rate, acid concentration, hydrodynamic force, and lithology.

4.1. Impact of Microstructure on the Dissolution Morphology. The dissolution surface morphology is controlled by rock mineral composition and reaction conditions. The difference in the crystal morphology of the rock leads to the difference in the dissolution of the crystal. When the external conditions are changed to speed up the overall reaction rate, different minerals will react with acids at different rates. After a period of reaction, uneven erosion of the surface will gradually appear and the regional differences will become more obvious.[26,27] The calcite percentage content of sample M is 96.72%, and the mineral composition was relatively single,

https://doi.org/10.1021/acsomega.3c08557
ACS Omega 2024, 9, 18922−18931

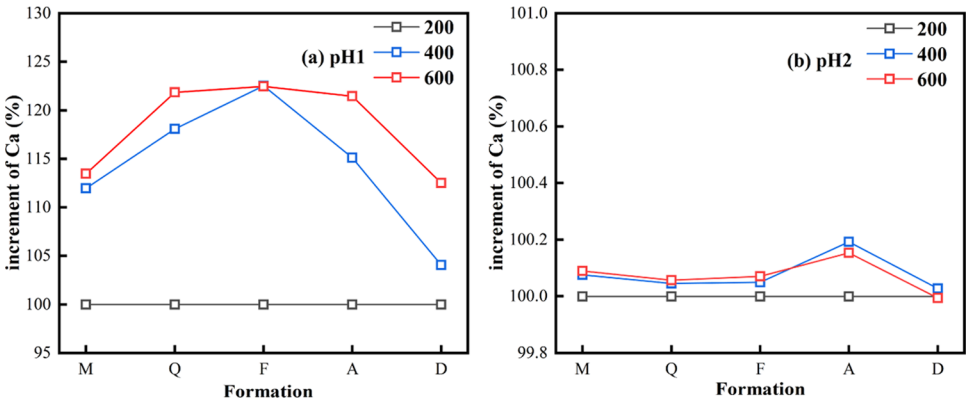

Figure 10. Percentage of Ca release increment calculated at 400 and 600 rpm using a sample at 200 rpm as reference.

which caused uniform dissolution and made the surface of the sample smooth and flat. The calcite of sample F accounted for 47.22%, and dolomite accounted for 51.93%. Dissolution differences in minerals result in uneven forms on the dissolved surface.[28] The connection between the contact surfaces of the different minerals was also weakened, resulting in easy peeling of rock surface materials. Therefore, the dissolution rate of the sample was more susceptible to the hydrodynamic changes. In addition, native defects in the crystal could lead to a microscopic pit etching morphology. The size of the crystal also had a certain influence on the reactivity of the rock (Figure 6a,b), and the reactivity of small crystals was greater than that of large crystals.[29−32]

4.2. Impact of Hydrodynamics on the Dissolution Rate. Under the condition of pH 1, the mass loss percent (R_c) of each group of samples increased to a certain extent with the increase in the disk speed (Figure 5a). According to the literature, enhanced hydrodynamic conditions increase the dissolution rate of calcite and dolomite, and a greater difference in flow rate could lead to a stronger dissolution.[33,34] The disk speed in the first gradient was from 200 to 400 rpm and in the second gradient was 400−600 rpm. The increment of the mass loss percent of the five groups of samples was 18.25−27.30% in the first gradient, while that in the second gradient was 1.95−8.14%. As shown in Figure 10, the percentage of Ca release increments calculated at 400 and 600 rpm was calculated using a sample at 200 rpm. In the pH 1 solution, the increment of Ca ion release was significantly correlated with the flow rate. The Ca release of sample M at 400 and 600 rpm was 11.97 and 13.47% higher than that at 200 rpm, respectively. The release of Ca from sample F at 400 and 600 rpm was 22.48% higher than that at 200 rpm. The release of Ca at 400 and 600 rpm in sample D was 4.07 and 12.52% higher than that at 200 rpm. In pH 2 solutions, Ca release also increased with increasing hydrodynamic conditions. However, the increment was small, with an average increment of less than 1% (Figure 10b). From both the increase in the dissolution rate and Ca and Mg content, the increase in the release of the second gradient was significantly smaller than that of the first gradient. Additionally, the increase in the two gradients was the same, but a significant difference in the increment of the dissolution amount was detected, indicating that the increase in the acid flow rate can promote the upper limit of the rock dissolution rate.

The mass loss percent (R_c) decreased with the decrease in the acid concentration.[23] As shown in Figures 5b and 10b, the mass loss percent and Ca dissolution of a part of the sample in the pH 2 solution were not increased with the increase in the disk speed. In the first gradient, the R_c increment of sample F was still the largest, and in the second gradient, only the R_c of samples M and Q increased, and the R_c of the remaining three groups of samples F, A, and D decreased by 1.24−2.87%. In acidic solutions, the mineral monolith made the mass loss percent and dissolution rate of the specimen regular. Due to the complex mineral composition of samples F, A, and D, an uneven distribution of minerals was induced, resulting in poor regularity of dissolution. When the acid concentration was high, the hydrodynamic effect enhanced the promotion effect on the rock dissolution more than that under the condition of low acid concentration.

4.3. Combined Impact. In the pH 1 solution, the chemical reaction rate (R) of each group of samples is illustrated in Figure 8b. Regression analysis of the relationship between reaction time and the chemical reaction rate (R) was conducted by using the logistic model ($R^2 > 0.990$). Under acidic conditions, an ideal correlation between the chemical reaction rate (R) and the acid−rock reaction time was extracted, and the acid−rock reaction time was one of the important influencing factors of the chemical reaction rate (R).[35] During the elapsed time, carbonate rocks were continuously dissolved and calcite dominated. If the acid solution was not replenished during the reaction, the reaction time increased and the concentration of reactants in the solution gradually decreased, which will lead to a decrease in the acid−rock reaction rate. Since all cutting surfaces of the rock sample were fresh-cut, the reaction rate was the largest at the beginning of the experiment, and the dissolution rate of calcium and magnesium was limited by the available fresh surface of the sample.[36] In the first 0.4 D of the reaction, the value of R is shown as sample Q was the largest, and sample A was the smallest. Among them, the CaO content of sample Q accounted for 54.93% and the MgO of sample A accounted for 13.33%, both of which accounted for the maximum values of each group. Previous works in the literature have reported that the high CaO content of rocks can promote dissolution and MgO has a strong inhibitory dissolution effect. In the pH 1 solution, the impact of the percentage content of CaO and MgO on the chemical reaction rate (R) is shown in Figure 11. The value of R decreased with an increase in the MgO content and increased with an increase in the CaO content. From the analysis of the compound content of samples Q and F, it was demonstrated that when the content of CaO was constant, the higher MgO content led to a lower chemical reaction rate (R), and less soluble carbonate rocks were observed in acids. From the compound content of samples M and Q, when the MgO content was constant, a higher CaO content indicates a greater value of R.[37]

https://doi.org/10.1021/acsomega.3c08557
ACS Omega 2024, 9, 18922−18931

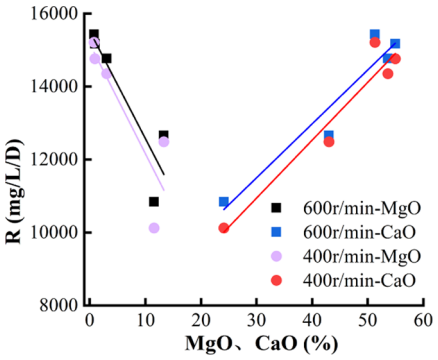

Figure 11. Impact of the percentage content of CaO and MgO on the chemical reaction rate (R).

As shown in Figure 12, the reaction sequence (m) and CaO/MgO (%) correspond to the exponential function relationship

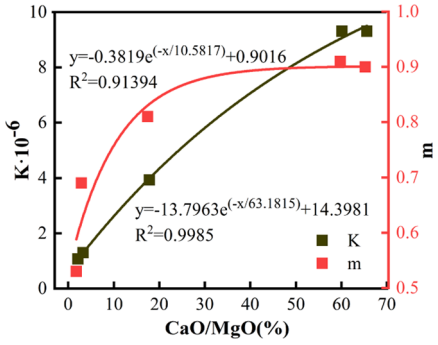

Figure 12. Reaction sequence (m) and CaO/MgO (%) correspond to the exponential function relationship.

(R^2 = 0.91394). The number of the reaction sequence (m) increased with the increase in the CaO/MgO ratio, and when 2 < CaO/MgO < 30, the value of m significantly changed in the range of 0.588−0.879. When 30 < CaO/MgO < 66, m was in the range of 0.879−0.901 and gradually tended to be stable. The difference in the CaO and MgO content in the sample had different degrees of promotion and inhibition of dissolution, so the relationship between CaO/MgO and chemical dissolution rate showed obvious segmentation characteristics. The increase in the reaction rate constant caused the acid−rock reaction rate to accelerate and the solubility to increase. The higher proportion of MgO in the rock indicates the existence of more obvious changes in the reaction sequence (m), and conversely, the reaction sequence (m) tended to be stable.

The main mineral composition of sample M was 96.72% calcite and 0.04% dolomite. The main minerals in sample M became 0.28% calcite and 99.65% dolomite. Therefore, the main dissolved components were $CaCO_3$ in limestone and $CaMg(CO_3)_2$ in dolomite. In acidic solutions, the solid solubility of $CaCO_3$ is greater than that of $CaMg(CO_3)_2$. There are significant differences in the dissolution rates of Ca and Mg in different types of carbonate rocks, which are related to the content of calcite and dolomite in the various layers. The difference in the dissolution between calcite and dolomite will form irregular dissolution channels, which is also responsible for the complexity of the underground dissolution system.

5. CONCLUSIONS

Dissolution experiments on carbonate cores from different formations have led to the following conclusions through basic physical and chemical tests, SEM tests, and correlation analyses:

(1) The mass loss rate (R_c) order of the rocks of the five carbonate formations was Maocaopu > Qingyan > Falang > Anshun > Dengying, and the initial chemical dissolution rate (R) order was Qingyan > Maocaopu > Falang > Dengying > Anshun.

(2) After being eroded by the acidic liquid, the macroscopic and microscopic morphologies of the cores changed significantly. Minerals were gradually dissolved, forming obvious dissolution pores and cracks. The changes in rock structure revealed the dissolution mechanism of carbonate under acidic conditions. In addition, the dissolution morphology of rocks was mainly affected by the composition and distribution of minerals, and the more single the composition, the more uniform the morphology.

(3) The relationship between CaO/MgO and chemical dissolution rate (R) showed obvious segmentation characteristics. When 2 < CaO/MgO < 30, m was in the range of 0.588−0.879, the change was obvious, while when 30 < CaO/MgO < 66, m was in the range of 0.879−0.901, and it gradually tended to be stabilized.

(4) In the dissolution process of carbonate rocks, there was an interaction between three conditions: liquid flow rate, acid concentration, and composition of rocks. The higher the acid concentration, the more significant the difference in dissolution caused by adjusting the liquid flow rate; the faster the liquid flow rate, the more the effect of the difference in carbonate composition on dissolution will be highlighted. The results of the study can provide some reference for tailings ponds and landfills in karst areas.

AUTHOR INFORMATION

Corresponding Author

Xuewei Chu − *College of Resources and Environmental Engineering, Guizhou University, Guiyang 550025 Guizhou, China*; Email: 28409807@qq.com

Authors

Jiaxin Zhang − *College of Resources and Environmental Engineering, Guizhou University, Guiyang 550025 Guizhou, China*; orcid.org/0009-0002-5211-7422

Hai Fu − *College of Resources and Environmental Engineering, Guizhou University, Guiyang 550025 Guizhou, China*

Qilin Zhang − *College of Resources and Environmental Engineering, Guizhou University, Guiyang 550025 Guizhou, China*

Shaokang Zong − *College of Resources and Environmental Engineering, Guizhou University, Guiyang 550025 Guizhou, China*

Complete contact information is available at: https://pubs.acs.org/10.1021/acsomega.3c08557

Notes

The authors declare no competing financial interest.

ACKNOWLEDGMENTS

This work was supported by the National Natural Science Foundation of China (42062016 and 42107080) and the

https://doi.org/10.1021/acsomega.3c08557
ACS Omega 2024, 9, 18922−18931

Science and Technology Fund of Guizhou Province (QKHZC[2020]4Y005).

REFERENCES

(1) Reddy, M. M.; Sherwood, S. I.; Doe, B. R. Materials Degradation Caused by Acid Rain. In *Limestone Marble Dissolution by Acid Rain An Onsite Weather*; American Chemical Society: Washington, DC, 1986; pp 226−238.
(2) Nyika, J.; Dinka, M.; Onyari, E. Effects of Landfill Leachate on Groundwater and Its Suitability for Use. *Mater. Today: Proc.* **2022**, *57*, 958−963.
(3) Labastida, I.; Armienta, M. A.; Lara-Castro, R. H.; Aguayo, A.; Cruz, O.; Ceniceros, N. Treatment of Mining Acidic Leachates with Indigenous Limestone, Zimapan Mexico. *J. Hazard. Mater.* **2013**, *262*, 1187−1195.
(4) Shi, B.; Li, X.; Hu, W.; Xi, B.; Liu, S.; Liu, D.; Xu, C.; Jia, Z.; Li, R. Environmental Risk of Tailings Pond Leachate Pollution: Traceable Strategy for Leakage Channel and Influence Range of Leachate. *J. Environ. Manage.* **2023**, *331*, No. 117341.
(5) Adabanija, M. A. Spatio-Temporal Monitoring of Leachates Dispersion beneath a Solid Wastes Dump in Basement Complex of Southwestern Nigeria. *J. Appl. Geophys.* **2023**, *210*, No. 104953.
(6) Noiriel, C.; Luquot, L.; Madé, B.; Raimbault, L.; Gouze, P.; van der Lee, J. Changes in Reactive Surface Area during Limestone Dissolution: An Experimental and Modelling Study. *Chem. Geol.* **2009**, *265* (1−2), 160−170.
(7) Pekala, M.; Wersin, P.; Pastina, B.; Lamminmäki, R.; Vuorio, M.; Jenni, A. Potential Impact of Cementitious Leachates on the Buffer Porewater Chemistry in the Finnish Repository for Spent Nuclear Fuel − A Reactive Transport Modelling Assessment. *Appl. Geochem.* **2021**, *131*, No. 105045, DOI: 10.1016/j.apgeochem.2021.105045.
(8) Kirstein, J.; Hellevang, H.; Haile, B. G.; Gleixner, G.; Gaupp, R. Experimental Determination of Natural Carbonate Rock Dissolution Rates with a Focus on Temperature Dependency. *Geomorphology* **2016**, *261*, 30−40.
(9) Leger, M.; Roubinet, D.; Jamet, M.; Luquot, L. Impact of Hydro-Chemical Conditions on Structural and Hydro-Mechanical Properties of Chalk Samples during Dissolution Experiments. *Chem. Geol.* **2022**, *594*, No. 120763, DOI: 10.1016/j.chemgeo.2022.120763.
(10) Arvidson, R. S.; Ertan, I. E.; Amonette, J. E.; Luttge, A. Variation in Calcite Dissolution Rates: A Fundamental Problem? *Geochim. Cosmochim. Acta* **2003**, *67* (9), 1623−1634.
(11) Covington, M. D.; Vaughn, K. A. Carbon Dioxide and Dissolution Rate Dynamics within a Karst Underflow-Overflow System, Savoy Experimental Watershed, Arkansas, USA. *Chem. Geol.* **2019**, *527*, No. 118689, DOI: 10.1016/j.chemgeo.2018.03.009.
(12) Phukan, M.; Vu, H. P.; Haese, R. R. Mineral Dissolution and Precipitation Reactions and Their Net Balance Controlled by Mineral Surface Area: An Experimental Study on the Interactions between Continental Flood Basalts and CO2-Saturated Water at 80 bar and 60 °C. *Chem. Geol.* **2021**, *559*, No. 119909, DOI: 10.1016/j.chemgeo.2020.119909.
(13) Finneran, D. W.; Morse, J. W. Calcite Dissolution Kinetics in Saline Waters. *Chem. Geol.* **2009**, *268* (1−2), 137−146.
(14) Békri, S.; Thovert, J. F.; Adler, P. M. Dissolution and Deposition in Fractures. *Eng. Geol.* **1997**, *48* (3−4), 283−308.
(15) Yoo, H.; Park, J.; Lee, Y.; Lee, J. An Experimental Investigation into the Effect of Pore Size Distribution on the Acid-Rock Reaction in Carbonate Acidizing. *J. Pet. Sci. Eng.* **2019**, *180*, 504−517.
(16) Li, Q.; Yi, X.; Lu, Y.; Li, G.; Chen, W. The Law of the Hydrogen Ion Diffusion Coefficient in Acid Rock Reaction. *J. Pet. Sci. Eng.* **2016**, *146*, 694−701.
(17) Li, Q.; Chen, W.; Lu, Y.; Xiao, Q. Etched Surface Morphology Analysis Experiments under Different Reaction Rates. *J. Pet. Sci. Eng.* **2019**, *172*, 517−526.
(18) Feng, P.; Ye, S.; Martys, N. S.; Bullard, J. W. Hydrodynamic Factors Influencing Mineral Dissolution Rates. *Chem. Geol.* **2020**, *541*, No. 119578, DOI: 10.1016/j.chemgeo.2020.119578.
(19) Bouissonnié, A.; Daval, D.; Marinoni, M.; Ackerer, P. From Mixed Flow Reactor to Column Experiments and Modeling: Upscaling of Calcite Dissolution Rate. *Chem. Geol.* **2018**, *487*, 63−75.
(20) Brand, A. S.; Feng, P.; Bullard, J. W. Calcite Dissolution Rate Spectra Measured by in Situ Digital Holographic Microscopy. *Geochim. Cosmochim. Acta* **2017**, *213*, 317−329.
(21) Ellis, B. R.; Peters, C. A. 3D Mapping of Calcite and a Demonstration of Its Relevance to Permeability Evolution in Reactive Fractures. *Adv. Water Resour.* **2016**, *95*, 246−253.
(22) Gonzalez-Herrera, R.; Vazquez-Mujica, P.; Canto-Ríos, J. Interactions of Waste Disposal Site Leachate with the Merida Karst Aquifer, Mexico. *J. Hydrol.* **2023**, *620*, No. 129436.
(23) Li, N.; Feng, Y.; Liu, P.; Luo, Z.; Zhao, L. Study of Acid−Rock Reaction Kinetics Under High Temperature and Pressure Conditions Based on the Rotating Disk Instrument. *Arab. J. Sci. Eng.* **2015**, *40* (1), 135−142.
(24) Pracný, P.; Faimon, J.; Všianský, D.; Přichystal, A. Evolution of Mg/Ca and Sr/Ca Ratios during the Experimental Dissolution of Limestone. *Chem. Geol.* **2019**, *523*, 107−120.
(25) Debure, M.; Lerouge, C.; Warmont, F.; Bocher, L.; Lundy, M.; Madé, B.; Grangeon, S. On the Interaction between Calcite and Dolomite: Insights from Gas and Aqueous Geochemistry and Mineralogical Characterization. *Chem. Geol.* **2021**, *559*, No. 119921.
(26) Noiriel, C.; Deng, H. Evolution of Planar Fractures in Limestone: The Role of Flow Rate, Mineral Heterogeneity and Local Transport Processes. *Chem. Geol.* **2018**, *497*, 100−114.
(27) Fischer, C.; Arvidson, R. S.; Lüttge, A. How Predictable Are Dissolution Rates of Crystalline Material? *Geochim. Cosmochim. Acta* **2012**, *98*, 177−185.
(28) Martyushev, D. A.; Govindarajan, S. K.; Li, Y.; Yang, Y. Experimental Study of the Influence of the Content of Calcite and Dolomite in the Rock on the Efficiency of Acid Treatment. *J. Pet. Sci. Eng.* **2022**, *208*, No. 109770.
(29) Xu, P.; Sheng, M.; Lin, T.; Liu, Q.; Wang, X.; Khan, W. A.; Xu, Q. Influences of Rock Microstructure on Acid Dissolution at a Dolomite Surface. *Geothermics* **2022**, *100*, No. 102324.
(30) Pollet-Villard, M.; Daval, D.; Fritz, B.; Knauss, K. G.; Schäfer, G.; Ackerer, P. Influence of Etch Pit Development on the Surface Area and Dissolution Kinetics of the Orthoclase (001) Surface. *Chem. Geol.* **2016**, *447*, 79−92.
(31) Rötting, T. S.; Luquot, L.; Carrera, J.; Casalinuovo, D. J. Changes in Porosity, Permeability, Water Retention Curve and Reactive Surface Area during Carbonate Rock Dissolution. *Chem. Geol.* **2015**, *403*, 86−98.
(32) Leger, M.; Luquot, L.; Roubinet, D. Role of Mineralogical, Structural and Hydrodynamic Rock Properties in Conduits Formation in Three Distinct Carbonate Rock Types. *Chem. Geol.* **2022**, *607*, No. 121008.
(33) Garcia-Rios, M.; Luquot, L.; Soler, J. M.; Cama, J. Influence of the Flow Rate on Dissolution and Precipitation Features during Percolation of CO2-Rich Sulfate Solutions through Fractured Limestone Samples. *Chem. Geol.* **2015**, *414*, 95−108.
(34) Xu, J.; Fan, C.; Teng, H. H. Calcite Dissolution Kinetics in View of Gibbs Free Energy, Dislocation Density, and PCO 2. *Chem. Geol.* **2012**, *322*−*323*, 11−18.
(35) Veetil, S. P.; Mucci, A.; Arakaki, T. Dolomite Dissolution Kinetics in Aqueous Solutions in the Presence of Organic and Inorganic Additives at 25 °C and PCO2 ∼ 1 atm. *Chem. Geol.* **2018**, *483*, 98−110.
(36) Saldi, G. D.; Causserand, C.; Schott, J.; Jordan, G. Dolomite Dissolution Mechanisms at Acidic PH: New Insights from High Resolution PH-Stat and Mixed-Flow Reactor Experiments Associated to AFM and TEM Observations. *Chem. Geol.* **2021**, *584*, No. 120521.
(37) Ivanishin, I. B.; Nasr-El-Din, H. A. Effect of Calcium Content on the Dissolution Rate of Dolomites in HCl Acid. *J. Pet. Sci. Eng.* **2021**, *202*, No. 108463.

https://doi.org/10.1021/acsomega.3c08557
ACS Omega 2024, 9, 18922−18931